THE JOURNAL OF PHYSICAL CHEMISTRY C

ARTICLE

pubs.acs.org/JPCC

Electromagnetic Field Shielding Polyurethane Nanocomposites Reinforced with Core−Shell Fe−Silica Nanoparticles

Jiahua Zhu,[†] Suying Wei,[‡] Neel Haldolaarachchige,[§] David P. Young,[§] and Zhanhu Guo[†,*]

[†]Integrated Composites Laboratory (ICL), Dan F. Smith Department of Chemical Engineering, Lamar University, Beaumont, Texas 77710, United States

[‡]Department of Chemistry and Biochemistry, Lamar University, Beaumont, Texas 77710, United States

[§]Department of Physics and Astronomy, Louisiana State University, Baton Rouge, Louisiana 70803, United States

ABSTRACT:

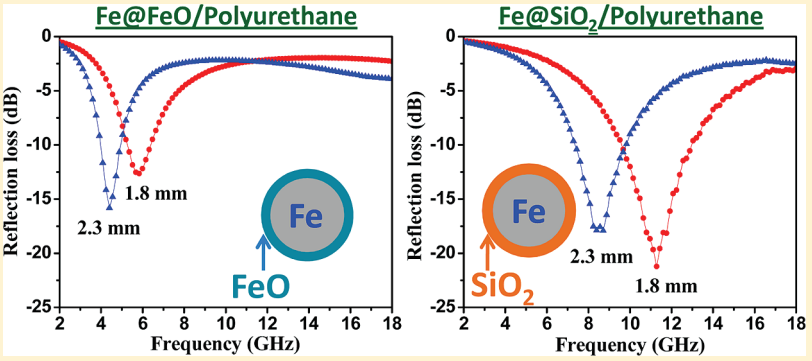

A modified Stöber method is introduced to synthesize Fe@SiO_2 nanoparticles (NPs) using 3-aminopropyltriethoxysilane (APTES) as a primer to render the metal particle surface compatible with silica. High-resolution transmission electron microscopy (HRTEM) and selected area electron diffraction (SAED) results indicate a highly crystalline iron core coated with a uniform layer of silica. Polyurethane (PU) nanocomposites filled with 71 wt % Fe@FeO and 71 wt % Fe@SiO_2 NPs are fabricated via a surface-initiated polymerization (SIP) method. The significantly increased coercivity of the resulting nanocomposites than that of the pure Fe@FeO NPs indicates that the NPs become magnetically harder after being dispersed in the PU matrix. Both Fe@SiO_2 NPs and Fe@SiO_2/PU nanocomposites exhibit better thermal stability and antioxidation capability than Fe@FeO and Fe@FeO/PU, respectively, owing to the barrier effect of the silica shell, revealed by the thermalgravimetric analysis (TGA). Meanwhile, the silica shell greatly reduces the eddy current loss and increases the anisotropy energy, which is essentially important to acquire higher reflection loss and broader absorption bandwidth for the microwave absorption. The Fe@SiO_2/PU nanocomposites show good electromagnetic wave absorption performance (reflection loss, RL < −20 dB) at high frequencies (11.3 GHz), while the best RL of Fe@FeO/PU is still larger than −20 dB even with a larger absorber thickness.

1. INTRODUCTION

Polymer nanocomposites (PNCs) have attracted considerable interest recently owing to their cost-effective processability, light weight, and tunable physiochemical properties. Deriving from the different composition, size, and morphology of the fillers, versatile unique properties are expected once they are combined with specific polymers. Astonishing progress has been made from different filler/polymer PNCs, such as the significantly enhanced mechanical strength and toughness of PNCs reinforced with carbon nanofibers (CNFs),[1,2] carbon nanotubes (CNTs),[3] and graphene;[4,5] the improved electrical conductivity in the conductive polymers (such as polyaniline and polypyrrole) incorporating semiconductive tungsten oxide nanoparticles (NPs) and nanorods;[6,7] and the improved thermal stability in PNCs with nanoclay as the fire-retardant materials.[8,9]

The fast development of the wireless communications has made the electromagnetic (EM) wave absorption materials even more attractive. The high-efficient EM absorption materials that possess broad absorption frequency, high absorption capacity, low weight, good thermal stability, and antioxidation capability are in great demand, and less work has been done until now.[10−13] PNCs are one of the best candidates which can be designed to meet the above requirements due to their adjustable properties in a wide range. Two groups of fillers are often introduced in a polymer to fabricate EM wave absorbers. The first group is carbon-based fillers, such as CNTs, graphite nanoplatelets (GNPs), and reduced graphene oxide (r-GO). For example, the shielding effectiveness of the CNTs/polystyrene foam composites containing 7 wt % CNTs was measured to be 18.2−19.3 dB over

Received: June 4, 2011
Revised: July 1, 2011
Published: July 05, 2011

Scheme 1. Schematic Illustration of Silica Coating on Fe@FeO NPs

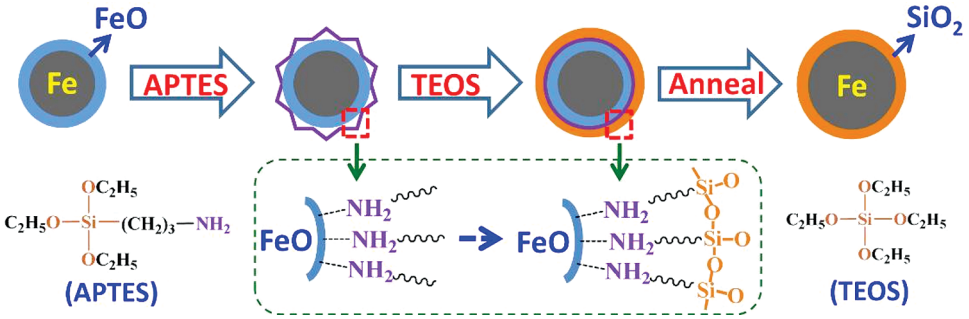

Scheme 2. Synthesis of PU

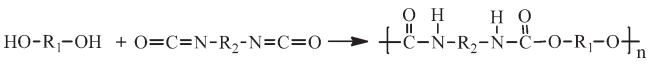

a frequency range of 8.2−12.4 GHz.[14] Even higher reflection loss of 24.27 dB at 15.3 GHz was observed in the CNTs/varnish composites with a CNT loading of 8 wt %.[15] GNP[16] and r-GO[17] were also studied as effective fillers for microwave absorption. The second group is metal and metal oxides, which attract more interest due to their unique permittivity and permeability property at microwave frequencies. Materials with large dielectric permittivity (ε), such as barium titanate ($BaTiO_3$, $\varepsilon \approx 1700$[18]) and zirconium titanate ($ZrTiO_3$, $\varepsilon \approx 2000$[18]) are widely studied for their microwave absorption properties.[11,19,20] However, high permittivity itself does not guarantee a high-efficiency microwave absorption, and high permeability is required especially at the high-frequency range. Therefore, ferromagnetic fillers, such as ferrites and carbonyl iron particles (CIPs), are often used to obtain high permeability; however, their permeabilities are drastically reduced at frequencies in the gigahertz range.[21,22] To obtain high reflection loss (RL) within a broad absorption frequency, researchers have paid attention to the modification of the filler structure and composition. For example, Wang et al. synthesized monodispersed hollow Fe_3O_4 nanospheres from a template-free process, and a minimum RL value of −42.7 dB was observed at 2.0 GHz with a thickness of 6.9 mm.[12] Zhu et al. coated a TiO_2 NP layer on the Fe_3O_4 nanotubes to obtain a core−shell structure,[23] which shows a minimum RL value of −20.6 dB at 17.28 GHz with an absorber thickness of 5 mm due to the reduced eddy current effect and improved anisotropy energy from TiO_2 shells.

Magnetic nanostructures of iron have been of great interest for EM wave absorption applications, which are supposed to retain high EM parameters in a high-frequency range due to their large saturation magnetization (M_s) and high Snoek's limit.[24−26] The Snoek's limit,[27] $\mu = F(f)$, is calculated from materials presenting cubic magnetocrystalline anisotropy in the absence of an external EM field. Above the limit, μ cannot have values. However, the weak magnetocrystalline anisotropy and attenuated permeability due to the eddy current phenomenon usually limit their applications at high frequencies.[28] Coating the iron particles with an insulating material is realized as an effective way to increase the surface anisotropy energy and reduce the eddy current effect.[29] Extensive studies have been conducted on the uniform coating of the metal NPs with silica shells.[30−33] The silica shell not only enhances the colloidal stability but also controls the distance between the core particles within the assemblies through shell thickness. Fe_2O_3[34] and Fe nanocubes[35] coated with silica have been reported for microwave absorption with a minimum RL of about −5 and −18.2 dB, respectively. However, a RL lower than −20 dB is required for real applications. Our recent result reports on the pure Fe NPs, and the microwave absorption bandwidth becomes narrow due to the eddy current loss though with a significant weight reduction.[36] To find suitable microwave absorptive PNCs with an enlarged RL and wide bandwidth is not a trial.

In this work, microwave absorptive polyurethane (PU) PNCs filled with Fe@SiO_2 NPs are reported with a much higher absorption capacity and broader absorption bandwidth at high frequency than the PU PNCs filled with the Fe@FeO NPs. The silica shell surrounding the Fe NPs is synthesized by a modified Stöber method with 3-aminopropyltriethoxysilane (APTES) as a primer to promote the deposition and adhesion of silica on the nanoparticle surface. The PU PNCs are fabricated with a surface-initiated polymerization (SIP) method. The thermal stability, electrical, magnetic, and microwave absorption properties are comparatively investigated in both PNC systems. The antioxidation capability is improved due to the protective silica shell.

2. EXPERIMENTAL SECTION

2.1. Materials. Core−shell structured Fe@FeO NPs, with an average size of 25 nm and shell thickness of 0.5 nm, are provided by QuantumSphere, Inc. 3-Aminopropyltriethoxysilane (APTES, 99%) is purchased from Sigma-Aldrich, and tetraethyl orthosilicate (TEOS, 99+%) is commercially available by Alfa Aesar. Ammonia (28%, lab grade), ethanol (99%), and tetrahydrofuran (THF, 99%) are purchased from Fisher scientific. All the chemicals are used without any further purification. The molecular structures of the APTES and TEOS, as well as the silica coating procedure, are shown in Scheme 1. The details of the silica coating are described in Section 2.2.

The PU is supplied by PRC-Desoto International, Inc., which contains three parts: part A and part C are accelerators and catalysts, and part B is the base compounds. The synthesis of PU is shown in Scheme 2.

2.2. Preparation of the Core−Shell NPs. In a typical procedure, Fe@FeO NPs (3 g) are ultrasonically dispersed in a mixture solution of ethanol (120 mL) and APTES (0.4 mL) for 30 min at 25 °C. After that, the suspension is kept still for 1 h to ensure the complexation between the amine groups of APTES and the nanoparticle surface. The silica shell growth follows the well-known Stöber method.[37] To be specific, the suspension is vigorously stirred at 500 rpm, and TEOS (1.8 mL) is rapidly

dx.doi.org/10.1021/jp2052536 |J. Phys. Chem. C 2011, 115, 15304–15310

injected into the suspension. Then, ammonia (12 mL) is added to the suspension by dropping slowly. The mechanical stirring is continued for 5 h, and then the particles are separated using a magnet. The particles are washed with ethanol and DI water three times and then dried in a vacuum oven overnight at room temperature. Finally, the dried particles are annealed at 650 °C for 2 h under an H_2/Ar (hydrogen ratio: ~5%) atmosphere to reduce the iron oxides to iron and complete the reaction from TEOS to silica.

2.3. Preparation of PU Nanocomposites. The Fe@FeO NPs (5 g) are initially mixed with a diluted mixture solution containing accelerators part A (0.36 g) and catalysts part C (0.40 g) and THF (20 mL), followed by 1 h sonication at room temperature to allow the adsorption of part A and C on the nanoparticle surface. Then, base compound part B (2.24 g) is added in the suspension, and the mixture suspension is mechanically stirred at 200 rpm in the ultrasonic bath for 1 h. The sonication is still on, and the temperature of the ultrasonic bath is controlled at 50 °C. The suspension is observed to become more viscous as the reaction proceeds. Finally, the viscous suspension is transferred into a mold and kept at room temperature for an additional 7 days to ensure the complete reaction and solvent evaporation. The final weight loading of the NPs is estimated to be 71 wt %, and the same weight of Fe@SiO_2 is used to synthesize the Fe@SiO_2/PU PNCs following the same procedures.

2.4. Characterization. The core@shell structures of the Fe@FeO and Fe@SiO_2 NPs are examined by transmission electron microscopy (TEM). The samples are observed in a FEI Tecnai G2 F20 with a field emission gun at a working voltage of 200 kV. All images are recorded as zero-loss images by excluding the contributions of inelastically scattered electrons using a Gatan Image Filter.

The thermal stability of the Fe@FeO, Fe@SiO_2, and their corresponding PNCs is studied by thermogravimetric analysis (TGA, TA Instruments TGA Q-500). TGA is conducted on these samples from 25 to 800 °C with an air flow rate of 60 mL/min and a heating rate of 10 °C/min.

A high resistance meter (Agilent 4339B) equipped with a resistivity cell (Agilent, 16008B) is used to measure the volume resistivity after inputting the sample thickness. This equipment allows resistivity measurement up to 10^{16} Ω. The source voltage is set at 0.1 V for all the samples. The reported values represent the mean value of eight measurements with a deviation less than 10%.

The magnetic properties of the PNCs at room temperature are carried out in a 9 T physical properties measurement system (PPMS) by Quantum Design.

The relative complex permeability and permittivity are measured using a transmission line technique. A washer-shaped specimen is cut from a thin sheet (~2 mm) of magnetic composites. The nominal outer and inner diameters of the specimen are 7.00 and 3.04 mm, respectively. The specimen is faced by abrading with a 320-grit SiC abrasive paper on a granite flat until a smooth and uniform surface is achieved. The specimen is then placed in a sample holder, which is located between the rigid beaded airline (APC-7) and the flexible coaxial airline (APC-7) that are connected to the network analyzer (HP model 8510B). The frequency generator is used to generate electromagnetic waves from 2 to 18 GHz. The permeability and permittivity are then deduced from the scattering parameters using a Nicholson–Ross algorithm.[38,39] The metal-backed reflection loss (MBRL) is calculated from the measured permittivity and permeability.

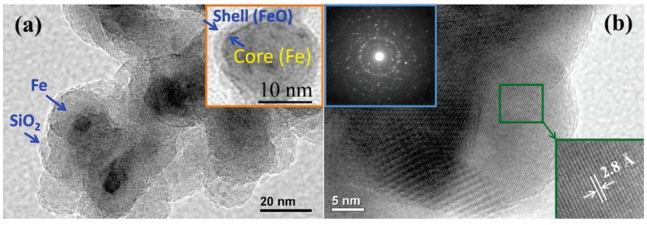

Figure 1. (a) TEM of Fe@SiO_2 core@shell structured NPs. The top inset exhibits the core@shell structure of the as-reveived NPs with a Fe core and FeO shell. (b) HRTEM of the Fe@SiO_2 NPs. The left inset shows the selected area electron diffraction (SAED) pattern of the NPs, and the right inset shows a lattice distance of 2.8 Å corresponding to the body-centered cubic iron.

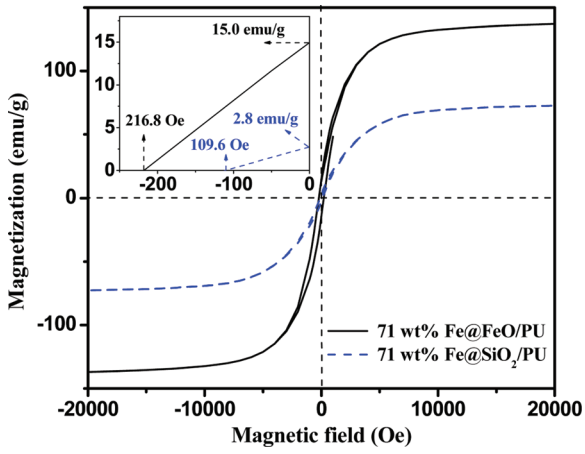

Figure 2. Hysteresis loops of the PU nanocomposites filled with 71 wt % Fe@FeO and Fe@SiO_2 NPs.

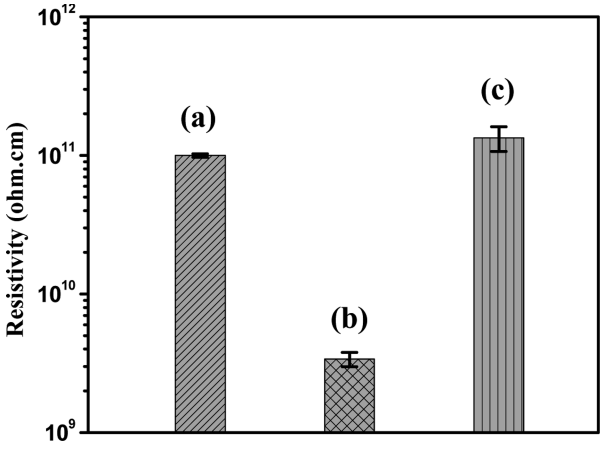

Figure 3. Resistivity of (a) pure PU, (b) 71 wt % Fe@FeO/PU, and (c) 71 wt % Fe@SiO_2/PU PNCs.

3. RESULTS AND DISCUSSION

3.1. TEM Investigation of the Core–Shell Structure. Figure 1(a) shows the microstructure of the Fe@SiO_2 core@shell NPs. The NPs are observed to be completely encapsulated by silica. The relatively dark areas in the image are iron NPs, and the light gray areas surrounding them are SiO_2, marked

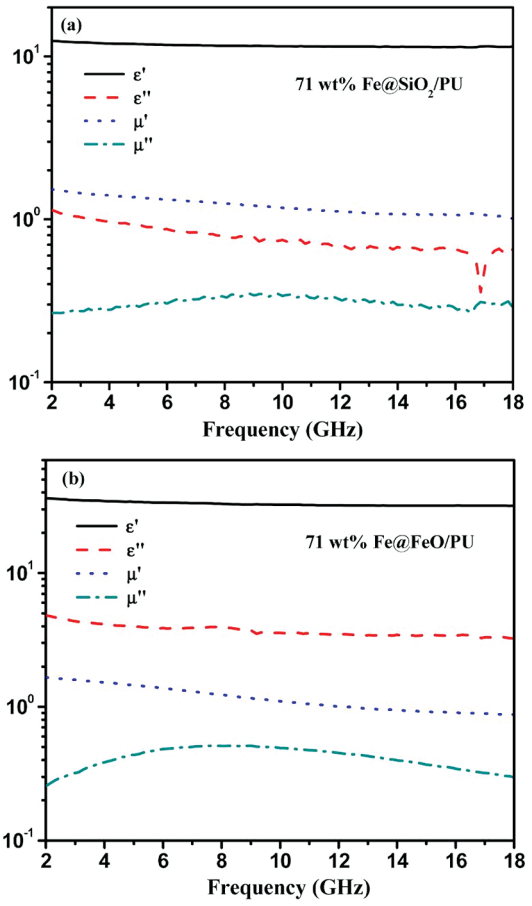

Figure 4. Permittivity and permeability vs frequency of the PNCs with a 71 wt % particle loading of (a) $Fe@SiO_2$ and (b) Fe@FeO.

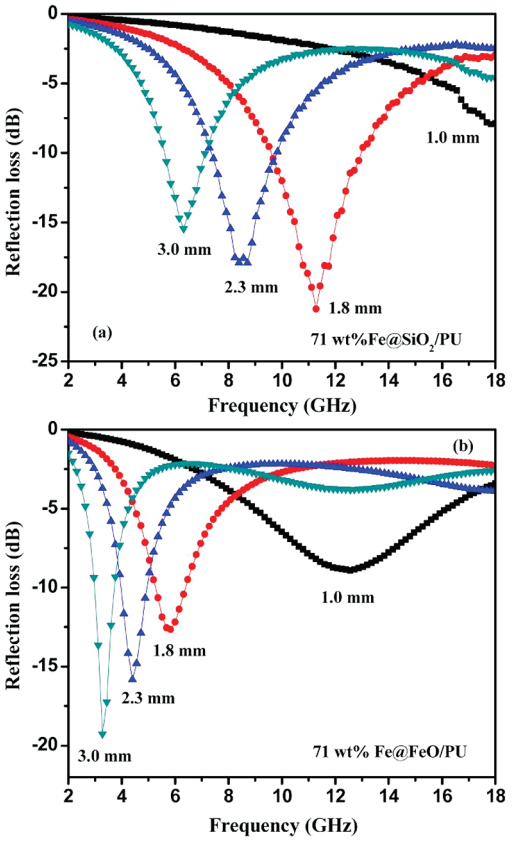

Figure 5. Dependence of RL on the thickness of the absorption layer within the frequency range of 2−18 GHz: (a) 71 wt % $Fe@SiO_2$/PU and (b) 71 wt % Fe@FeO/PU PNCs.

with arrows in Figure 1(a). The as-received NPs are core@shell structured with a FeO shell thickness of about 1 nm (inset of Figure 1a). To ensure the reduction of the iron oxide shell to iron during the annealing, a high-resolution TEM image of the $Fe@SiO_2$ NPs is taken (Figure 1(b)). Focusing on the edge of the $Fe@SiO_2$ NPs, the iron core extends its crystalline structure to the end of the interface and is covered by a thin layer of amorphous silica, and the FeO shell disappears in the $Fe@SiO_2$ NPs. This observation confirms that the FeO shell has been reduced to Fe during the annealing. The selected area electron diffraction (SAED) pattern (left inset of Figure 1(b)) shows the crystalline structure of the iron core, and the lattice fringe space of 2.8 Å (bottom inset of Figure 1(b)) corresponds to the typical lattice distance of the body-centered cubic iron.[40,41]

3.2. Magnetic and Electrical Properties. Figure 2 shows the magnetic hysteresis loops of the PNCs filled with the same loading of Fe@FeO and $Fe@SiO_2$ NPs. Both PNCs are saturated at a relatively high magnetic field. The $Fe@SiO_2$/PU PNCs exhibit lower saturated magnetization (M_s) of 72.6 emu/g than that of the Fe@FeO/PU PNCs (137.1 emu/g), which is due to the silica shell with an almost zero M_s in the $Fe@SiO_2$ NPs. Much larger coercivities (H_c) of 216.8 and 109.6 Oe are observed in the PNCs filled with Fe@FeO and $Fe@SiO_2$ NPs, respectively. The coercivity of the Fe@FeO NPs is reported as 62.3 Oe in our previous work,[42] and the enhanced H_c of the PNCs is due to the decreased interparticle dipolar interaction, which arises from the enlarged internanoparticle distance for the single domain NPs,[43,44] as compared to the close contact of the Fe@FeO NPs.

Figure 3 shows the volume resistivity of the pure PU and its PNCs filled with 71 wt % Fe@FeO and 71 wt % $Fe@SiO_2$ NPs, respectively. The pure PU shows a volume resistivity of about 10^{11} ohm cm^{-1}, which is in good agreement with the other reported value.[45] The 71 wt % Fe@FeO/PU PNCs still behave like an insulator even though a significant resistivity reduction as high as 96.6% is observed. Comparing with the prominent geometrical models created by Kirkpatrick[46] and Zallen,[47] the required minimum touching spherical particles is 16 vol %. This value is in approximate agreement with the most experimental observations that the critical volume fraction is between 5 and 20 vol % for polymer composites filled with powdery materials.[42] However, the much higher spherical Fe@FeO NP loading of 71 wt % (24.8 vol %, estimated from $\rho_{Fe@FeO} = 7.80$ g/cm^3 and $\rho_{PU} = 1.05$ g/cm^3) is above the critical volume fraction, and the Fe@FeO/PU PNCs still remain insulated. This nonconductive behavior is attributed to the compact insulating PU layer on the nanoparticle surface from the SIP method, which prevents the direct contact among the Fe@FeO NPs. After coating the Fe@FeO NPs with a silica shell, the corresponding PNCs exhibit even higher volume resistivity than that of pure PU, which is due to the higher resistance of the silica coating (10^{14}−10^{16} ohm cm^{-1}) on the NPs.[48]

3.3. Microwave Absorption. Figure 4 shows the frequency-dependent real part (ε') and imaginary part (ε'') of the relative complex permittivity ($\varepsilon_r = \varepsilon' - j\varepsilon''$) and the real part ($\mu'$)

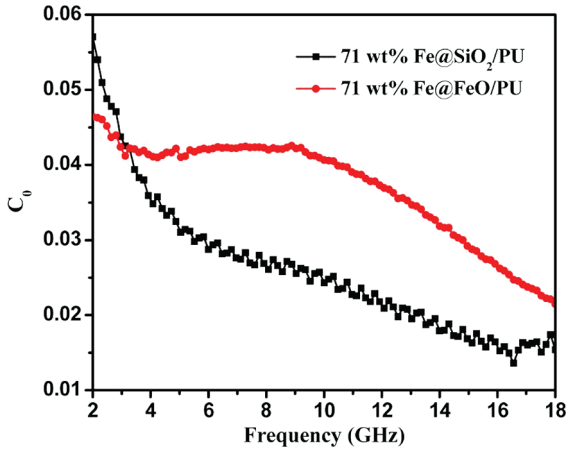

Figure 6. C_0-f curves of Fe@SiO_2/PU and Fe@FeO/PU PNCs.

and imaginary part (μ'') of the relative complex permeability ($\mu_r = \mu' - j\mu''$) for the Fe@SiO_2 (Figure 4(a)) and Fe@FeO (Figure 4(b)) core−shell NP filled PU PNCs, respectively. The ε' value experiences a slight decrease within the frequency range of 2−18 GHz in both composite systems. The PNCs reinforced with Fe@SiO_2 particles show the ε' between 11.5 and 12.5, while a significantly higher ε' value of 31.8−36.3 is observed from the Fe@FeO/PU PNCs. The ε'' shows a slight decrease with increasing frequency for both PNCs (Figure 4(a)). It is interesting to observe that the μ' and μ'' curves of both PNCs are quite similar to each other. The μ' value slightly decreases from 2 to 18 GHz, which is in the range of 1.53−1.02 and 1.66−0.88 for the Fe@SiO_2/PU and Fe@FeO/PU PNCs, respectively. This is favorable for a microwave surface impedance match because the wavelength in the microwave absorber decreases with increasing frequency.[49] The spectra of μ'' show a convex curve, which is recognized as the frequency dispersion phenomena. The frequency dispersion of the PNCs is attributed to the magnetic resonance of the NPs and domain wall turning.[22,49] The nonmagnetic silica coating on the magnetic NPs enhances the effective reluctance of the PNCs and thus results in the relatively weak frequency dispersion phenomena (relative flat curve of μ'' in Figure 4a than in Figure 4b).

To acquire the microwave absorption properties, the MBRL is calculated according to transmission line theory.[50] The RL of EM radiation, under normal wave incidence at the surface of a single-layer material backed by a perfect conductor, can be defined as[51]

$$RL = 20 \log_{10}\left|\frac{Z-1}{Z+1}\right| \quad (1)$$

where Z is the input impedance at the interface of free space and material

$$Z = \sqrt{\frac{\mu}{\varepsilon}}\tanh\left(-i\frac{2\pi f d}{c}\sqrt{\mu\varepsilon}\right) \quad (2)$$

where f is the frequency of the electromagnetic wave; d is the thickness of the absorbing material; ε and μ are the relative complex permittivity and permeability; and c is the velocity of electromagnetic waves in free space. The RL of both the Fe@SiO_2/PU and the Fe@FeO/PU PNCs with the sample thickness varied from 1 to 3 mm is calculated (Figure 5). The

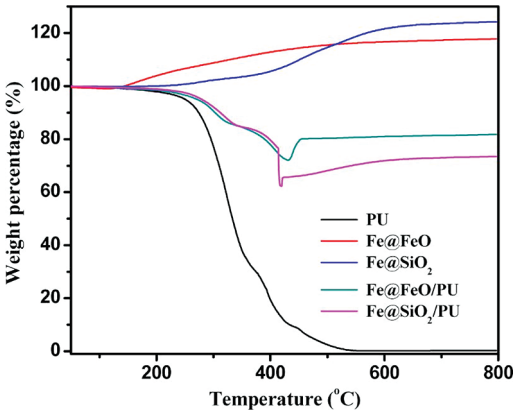

Figure 7. TGA curve of the PNCs filled with different particles.

minimum RL reaches −21.2 dB at 11.3 GHz for the Fe@SiO_2/PU absorber with a thickness of 1.8 mm. Moreover, the absorption bandwidth with the RL below −10 dB is up to 7.5 GHz (from 5.5 to 13.0 GHz). For the Fe@FeO/PU PNCs, the absorption bandwidth of RL below −10 dB is only 3.4 GHz (from 3.0 to 6.4 GHz), and the minimum RL is not able to reach −20 dB even when the absorber thickness is increased to 3 mm. Since the Fe@SiO_2/PU PNCs obtain the higher relative RL, a broader absorption bandwidth, and a smaller absorber thickness than those of the Fe@FeO/PU PNCs, these Fe@SiO_2/PU PNCs are poised to be very promising for new types of EM wave absorptive materials. On the basis of the results observed above, it is indicated that the silica shell plays a positive role in the microwave absorption properties of the Fe@SiO_2/PU PNCs. The results are comparable to the results obtained from Fe_3O_4−TiO_2 core−shell nanotubes.[23] The reasons can be explained from two aspects: the decrease of the eddy current effect and the increase of the anisotropy energy of the Fe@SiO_2 core−shell NPs. For the ferromagnetic absorber, the EM absorption properties are usually subjected to degradation caused by the eddy current effect in the high-frequency region. The eddy current loss can be evaluated by eq 3[52]

$$\mu'' \approx 2\pi\mu_0(\mu')^2\sigma \cdot d^2 f/3 \quad (3)$$

where σ ($S \cdot m^{-1}$) is the electrical conductivity and μ_0 ($H \cdot m^{-1}$) is the permeability in vacuum. If the reflection loss results from the eddy current loss effect, the values of C_0 ($C_0 = \mu''(\mu')^{-2}f^{-1}$) are constant when the frequency is changing. Figure 6 shows the C_0-f curves of both Fe@FeO/PU and Fe@SiO_2/PU PNCs. For the Fe@FeO/PU PNCs, the value of C_0 is almost constant within the frequency range from 3 to 9 GHz; after that it decrease with increasing frequency. However, the C_0 decreases continuously from 2 to 16.5 GHz after coating silica on the Fe@FeO NPs. This result implies that the Fe@FeO/PU PNCs have a significant eddy current effect, which is reduced after coating a silica layer on the NP surface.

The other reason for the better microwave absorptive performance in the Fe@SiO_2/PU PNCs is ascribed to the enhanced anisotropic energy (H_a), which can be expressed in eq 4.

$$H_a = 4|K_1|/3\mu_0 M_s \quad (4)$$

where $|K_1|$ is the anisotropic coefficient. The M_s value of the Fe@SiO_2/PU PNCs is about half of the Fe@FeO/PU PNCs (Figure 2). Therefore, the anisotropic energy is higher for the

Fe@SiO_2/PU PNCs. The higher anisotropic energy is helpful to the improvement of EM absorption properties especially at high frequency.[53−55]

3.4. Thermalgravimetric Analysis. The thermal stability of the pure PU, Fe@FeO, Fe@SiO_2, and their composites is shown in Figure 7. The pure PU begins to decompose at around 250 °C and burns out at 550 °C. Both NPs exhibit a significant weight increase in the final stage owing to the oxidation in air at elevated temperatures. The Fe@FeO NPs experience a slight weight loss at below 100 °C, which is due to the adsorbed moisture on the particle surface. The weight of the NPs begins to increase at ∼130 °C. After coating with a silica shell, the NPs are protected, and the oxidation temperature increases to about 215 °C. The higher weight increase of the Fe@SiO_2 at high temperature range (500−800 °C) than that of Fe@FeO is primarily due to the reduction of the FeO shell to Fe during the annealing process, and then the total oxygen content in iron oxide accounts for the final weight increase after oxidation. The similar weight increase induced by iron oxidation is also observed in the composites. Accompanied by the decomposition of PU, the degradation curves of composites are more complicated, especially within the temperature range of 300−500 °C. The oxidation process for the Fe@FeO/PU is finished at ∼460 °C, which shows a flat curve afterward. However, after coating a silica layer, the oxidation process is much slower, and the complete oxidation is delayed to 650 °C, which further confirms the protective behavior of the silica shell.

4. CONCLUSION

Core@shell structured Fe@SiO_2 NPs have been prepared using a modified Stöber method. The silica-coated NPs and the corresponding PNCs are more thermally stable based on the TGA results. The insulating silica layer on the magnetic particle surface is helpful to improve the resistivity of the PNCs, which is essentially important to acquire a high RL and broad absorption bandwidth for the microwave absorption. The silica shell greatly reduces the eddy current loss and increases the anisotropy energy, which are proved to be essentially important to acquire high RL and broad absorption bandwidth for the microwave absorption. The Fe@SiO_2/PU PNC absorber with 1.8 mm thickness shows a good electromagnetic wave absorption performance (RL < −20 dB) at a high frequency of 11.3 GHz, while the best RL of the Fe@FeO/PU PNC absorber is still lower than −20 dB, even increasing the absorber thickness to 3 mm.

AUTHOR INFORMATION

Corresponding Author

*E-mail: zhanhu.guo@lamar.edu. Phone: (409) 880-7654. Fax: (409) 880-2197.

ACKNOWLEDGMENT

This project is partially supported by the National Science Foundation - Nanoscale Interdisciplinary Research Team and Materials Processing and Manufacturing (CMMI 10-30755). D. P. Young acknowledges support from the NSF under Grant No. DMR 10-05764.

REFERENCES

(1) Al-Saleh, M. H.; Sundararaj, U. *Carbon* **2009**, *47*, 2–22.
(2) Zhu, J.; Wei, S.; Ryu, J.; Budhathoki, M.; Liang, G.; Guo, Z. *J. Mater. Chem.* **2010**, *20*, 4937–4948.
(3) Coleman, J. N.; Khan, U.; Blau, W. J.; Gun'ko, Y. K. *Carbon* **2006**, *44*, 1624–1652.
(4) Xu, Z.; Gao, C. *Macromolecules* **2010**, *43*, 6716–6723.
(5) RamanathanT; Abdala, A. A.; StankovichS; Dikin, D. A.; Herrera Alonso, M.; Piner, R. D.; Adamson, D. H.; Schniepp, H. C.; ChenX; Ruoff, R. S.; Nguyen, S. T.; Aksay, I. A.; Prud'Homme, R. K.; Brinson, L. C. *Nat. Nanotechnol.* **2008**, *3*, 327–331.
(6) Zhu, J.; Wei, S.; Zhang, L.; Mao, Y.; Ryu, J.; Karki, A. B.; Young, D. P.; Guo, Z. *J. Mater. Chem.* **2011**, *21*, 342–348.
(7) Zhu, J.; Wei, S.; Zhang, L.; Mao, Y.; Ryu, J.; Mavinakuli, P.; Karki, A. B.; Young, D. P.; Guo, Z. *J. Phys. Chem. C* **2010**, *114*, 16335–16342.
(8) Duquesne, S.; Jama, C.; Le Bras, M.; Delobel, R.; Recourt, P.; Gloaguen, J. M. *Compos. Sci. Technol.* **2003**, *63*, 1141–1148.
(9) Uhl, F. M.; Morgan, A. B.; Wilkie, C. A. *Chem. Mater.* **2001**, *13*, 4649–4654.
(10) Toneguzzo, P.; Viau, G.; Acher, O.; Fiévet-Vincent, F.; Fiévet, F. *Adv. Mater.* **1998**, *10*, 1032–1035.
(11) Guo, Z.; Lee, S. E.; Kim, H.; Park, S.; Hahn, H. T.; Karki, A. B.; Young, D. P. *Acta Mater.* **2009**, *57*, 267–277.
(12) Wang, F.; Liu, J.; Kong, J.; Zhang, Z.; Wang, X.; Itoh, M.; Machida, K. *J. Mater. Chem.* **2011**, *21*, 4314–4320.
(13) Chiu, S.-C.; Yu, H.-C.; Li, Y.-Y. *J. Phys. Chem. C* **2010**, *114*, 1947–1952.
(14) Yang, Y.; Gupta, M. C.; Dudley, K. L.; Lawrence, R. W. *Nano Lett.* **2005**, *5*, 2131–2134.
(15) Fan, Z.; Luo, G.; Zhang, Z.; Zhou, L.; Wei, F. *Mater. Sci. Eng., B* **2006**, *132*, 85–89.
(16) Lee, Sang-Eui; Choi, Oyoung; Hahn, H. T. *J. Appl. Phys.* **2008**, *104*, 033705.
(17) Wang, C.; Han, X.; Xu, P.; Zhang, X.; Du, Y.; Hu, S.; Wang, J.; Wang, X. *Appl. Phys. Lett.* **2011**, *98*, 072906.
(18) Barber, P.; Balasubramanian, S.; Anguchamy, Y.; Gong, S.; Wibowo, A.; Gao, H.; Ploehn, Harry J.; Loye, H.-C. z. *Materials* **2009**, *2*, 1697–1733.
(19) Abbas, S. M.; Dixit, A. K.; Chatterjee, R.; Goel, T. C. *Mater. Sci. Eng., B* **2005**, *123*, 167–171.
(20) Azough, F.; Freer, R.; Wang, C. L.; Lorimer, G. W. *J. Mater. Sci.* **1996**, *31*, 2539–2549.
(21) Haijun, Z.; Zhichao, L.; Chengliang, M.; Xi, Y.; Liangying, Z.; Mingzhong, W. *Mater. Sci. Eng., B* **2002**, *96*, 289–295.
(22) Singh, P.; Babbar, V. K.; Razdan, A.; Srivastava, S. L.; Goel, T. C. *Mater. Sci. Eng., B* **2000**, *78*, 70–74.
(23) Zhu, C.-L.; Zhang, M.-L.; Qiao, Y.-J.; Xiao, G.; Zhang, F.; Chen, Y.-J. *J. Phys. Chem. C* **2010**, *114*, 16229–16235.
(24) Yoshida, S.; Sato, M.; Sugawara, E.; Shimada, Y. *J. Appl. Phys.* **1999**, *85*, 4636.
(25) Snoek, J. L. *Physica* **1948**, *14*, 207–217.
(26) Zhu, J.; Wei, S.; Li, Y.; Sun, L.; Haldolaarachchige, N.; Young, D. P.; Southworth, C.; Khasanov, A.; Luo, Z.; Guo, Z. *Macromolecules* **2011**, *44*, 4382–4391.
(27) Chikazumi, S. *Physics of Magnetism*; Krieger: Boca Raton, FL, 1998.
(28) Sun, X.-C.; Nava, N. *Nano Lett.* **2002**, *2*, 765–769.
(29) Zhang, X. F.; Dong, X. L.; Huang, H.; Lv, B.; Lei, J. P.; Choi, C. J. *J. Phys. D: Appl. Phys.* **2007**, *40*, 5383.
(30) Graf, C.; Vossen, D. L. J.; Imhof, A.; van Blaaderen, A. *Langmuir* **2003**, *19*, 6693–6700.
(31) Kobayashi, Y.; Katakami, H.; Mine, E.; Nagao, D.; Konno, M.; Liz-Marzán, L. M. *J. Colloid Interface Sci.* **2005**, *283*, 392–396.
(32) Santra, S.; Tapec, R.; Theodoropoulou, N.; Dobson, J.; Hebard, A.; Tan, W. *Langmuir* **2001**, *17*, 2900–2906.
(33) Lu, Y.; Yin, Y.; Mayers, B. T.; Xia, Y. *Nano Lett.* **2002**, *2*, 183–186.
(34) Guo, X.; Deng, Y.; Gu, D.; Che, R.; Zhao, D. *J. Mater. Chem.* **2009**, *19*, 6706–6712.
(35) Ni, X.; Zheng, Z.; Hu, X.; Xiao, X. *J. Colloid Interface Sci.* **2010**, *341*, 18–22.
(36) Guo, Z.; Park, S.; Hahn, H. T.; Wei, S.; Moldovan, M.; Karki, A. B.; Young, D. P. *J. Appl. Phys.* **2007**, *101*, 09M511.

(37) Stöber, W.; Fink, A.; Bohn, E. *J. Colloid Interface Sci.* **1968**, *26*, 62–69.
(38) Nicolson, A. M.; Ross, G. F. *IEEE Trans. Instrum. Meas.* **1970**, *IM-19*, 377–382.
(39) Nicolson, A. M.; Ross, G. F. *IEEE Trans. Instrum. Meas.* **1968**, *17*, 395–402.
(40) Wood, J. H. *Phys. Rev.* **1962**, *126*, 517.
(41) Bagayoko, D.; Callaway, J. *Phys. Rev. B* **1983**, *28*, 5419.
(42) Zhu, J.; Wei, S.; Ryu, J.; Sun, L.; Luo, Z.; Guo, Z. *ACS Appl. Mater. Interfaces* **2010**, *2*, 2100–2107.
(43) Guo, Z.; Lei, K.; Li, Y.; Ng, H. W.; Prikhodko, S.; Hahn, H. T. *Compos. Sci. Technol.* **2008**, *68*, 1513–1520.
(44) Guo, Z.; Lin, H.; Karki, A. B.; Wei, S.; Young, D. P.; Park, S.; Willis, J.; Hahn, T. H. *Compos. Sci. Technol.* **2008**, *68*, 2551–2556.
(45) Kim, H.; Miura, Y.; Macosko, C. W. *Chem. Mater.* **2010**, *22*, 3441–3450.
(46) Kirkpatrick, S. *Rev. Mod. Phys.* **1973**, *45*, 574.
(47) Zallen, R. *The Physics of Amorphous Solids*; Wiley: New York, 1983.
(48) Sze, S. M. *Physics of semiconductor devices*; Wiley Eastern Ltd.: New York, 1981.
(49) Yang, Y.; Zhang, B.; Xu, W.; Shi, Y.; Zhou, N.; Lu, H. *J. Magn. Magn. Mater.* **2003**, *265*, 119–122.
(50) Miles, P. A.; Westphal, W. B.; Von Hippel, A. *Rev. Mod. Phys.* **1957**, *29*, 279.
(51) Michielssen, E. S., J.; Ranjithan, S.; Mittra, R. *IEEE Trans.* **1993**, *41*, 1024–1030.
(52) Wu, M.; Zhang, Y. D.; Hui, S.; Xiao, T. D.; Ge, S.; Hines, W. A.; Budnick, J. I.; Taylor, G. W. *Appl. Phys. Lett.* **2002**, *80*, 4404.
(53) Che, R. C.; Zhi, C. Y.; Liang, C. Y.; Zhou, X. G. *Appl. Phys. Lett.* **2006**, *88*, 033105.
(54) Liu, X. G.; Geng, D. Y.; Meng, H.; Shang, P. J.; D., Z. Z. *Appl. Phys. Lett.* **2008**, *92*, 173117.
(55) Che, R. C.; Peng, L. M.; Duan, X. F.; Chen, Q.; Liang, X. L. *Adv. Mater.* **2004**, *16*, 401–405.